



**HAL**  
open science

## A description of internal erosion by suffusion and induced settlements on cohesionless granular matter

Luc Sibille, Didier Marot, Yacine Sail

### ► To cite this version:

Luc Sibille, Didier Marot, Yacine Sail. A description of internal erosion by suffusion and induced settlements on cohesionless granular matter. *Acta Geotechnica*, 2015, 10 (6), pp.735-748. 10.1007/s11440-015-0388-6 . hal-01299663

**HAL Id: hal-01299663**

<https://hal.univ-grenoble-alpes.fr/hal-01299663v1>

Submitted on 8 Apr 2016

**HAL** is a multi-disciplinary open access archive for the deposit and dissemination of scientific research documents, whether they are published or not. The documents may come from teaching and research institutions in France or abroad, or from public or private research centers.

L'archive ouverte pluridisciplinaire **HAL**, est destinée au dépôt et à la diffusion de documents scientifiques de niveau recherche, publiés ou non, émanant des établissements d'enseignement et de recherche français ou étrangers, des laboratoires publics ou privés.

# **A description of internal erosion by suffusion and induced settlements on cohesionless granular matter**

**Luc Sibille<sup>1,2,\*</sup> • Didier Marot<sup>1</sup> • Yacine Sail<sup>1</sup>**

## **Abstract**

Cohesionless granular matter subjected to internal flow can incur an internal erosion by suffusion characterized by a migration of its finest constituting particles. A series of suffusion tests is performed on assemblies of gap graded glass beads using a large oedo-permeameter device. Two successive processes of erosion can be observed during the tests. First, a suffusion process is characterized by a progressive and diffuse migration of fine particles over a long time period. The second process, induced by the first one, is characterized by a strong migration over a short time period (blowout of fine particles) and produces rapidly large settlement of specimen. Time series of hydraulic conductivity, longitudinal profile of specimen density, eroded mass and axial deformation are analyzed. The initial content of fine particles and the history of hydraulic loading appear as key parameters in the suffusion development. To characterize the suffusion development, erosion rate is investigated according to the power expended by the seepage flow, and a new law of erosion by suffusion is proposed.

**Keywords:** internal erosion • suffusion • flow power • erodimeter • granular media

## **1 Introduction**

The water seepage within earth structures, such as embankments, dams or dikes, can generate a detachment and a transport of particles from the soil constituting the structure or its foundation. This phenomenon named internal erosion can be detailed in four types (Fell and Fry, 2007; Bonelli, 2012): 1) erosion in concentrated leak, i.e. the water erodes a crack, a hole

<sup>1</sup>Nantes Université, Institut GeM, UN-ECN-CNRS, 44600 Saint-Nazaire, France.

<sup>2</sup>Université Grenoble Alpes, CNRS, 3SR, F-38000 Grenoble, France.

\* Corresponding author, e-mail : luc.sibille@3sr-grenoble.fr

or a hollow, 2) backward erosion mainly appears in soil of foundations and progresses from a free surface on the downstream side of earth structure, 3) suffusion also named internal instability, which takes place inside the soil matrix and 4) contact erosion occurs at an interface between a fine soil layer and another layer made of a coarser soil. In this last case, due to the important difference in the hydraulic conductivity respectively in the fine and coarse soil layers, the water flow is concentrated within the coarse soil. This paper deals with suffusion process which may develop in the bulk of a soil volume when the particle size grading and the porosity are such that the fine fraction of the soil can migrate through the skeleton formed by the coarse fraction (i.e. when fine particles can pass through the constrictions of the granular skeleton of the coarse fraction). Suffusion is thus defined as the detachment, the transport, and possibly the redeposition of fine particles in the pore space between the coarser particles.

With the objective to evaluate the likelihood of suffusion initiation, several geometric criteria based on the grain size distribution have been proposed in the literature (among others Burenkova, 1993; Kenney and Lau, 1985). However, according to Li and Fannin (2008) and also Wan and Fell (2008), the most widely used geometric methods are conservative. Nowadays research works are still carried out concerning such geometric criteria, they aim for instance to take into account rather the size distribution of constrictions than directly the grain size distribution (Vincens *et al.*, 2014); or the degree of interlocking of fines by neighbouring particles in relation with their involvement in the stress transmission by the granular skeleton (Shire and O'Sullivan, 2013; Moffat and Herrera, 2014).

Moreover, even if the transport of particles is geometrically feasible, the action of the hydraulic flow must be sufficient for detaching some particles from the soil (Kovacs, 1981).

The hydraulic loading on soil particles is often described by three distinct approaches: the hydraulic gradient (Skempton and Brogan, 1994; Li, 2008), the hydraulic shear stress (Reddi *et al.*, 2000), and the pore velocity (Perzmaier, 2007). The critical values of all these three parameters can be used to characterize the suffusion initiation. Suffusion tests on clayey sand (Marot *et al.*, 2012a) and on cohesionless granular matter (Li, 2008) show that the critical hydraulic gradient decreases with the length of tested specimens. It is worth noting that this dependence of critical hydraulic gradient on the size of tested samples constitutes a drawback with respect to the risk management in the field. Consequently, how should the critical hydraulic gradient be scaled from laboratory tests to large field's problems?

Moreover suffusion may be accompanied by the filtration of some detached particles causing a redistribution of the porosity. This can induce a clogging process within the soil and may

finally result in a decrease of the hydraulic conductivity (Reddi *et al.*, 2000; Bendahmane *et al.*, 2008; Marot *et al.*, 2009). Therefore, variations of both seepage velocity and pressure gradient have to be taken into account to evaluate the hydraulic loading. With such objective and in the case of cohesive soils, Reddi *et al.* (2000) proposed to represent the porous medium by a system of parallel capillary tubes. Thanks to this modelling of porous media, the hydraulic shear stress along the horizontal capillary tube system can be expressed in terms of pressure gradient, porosity and intrinsic permeability of the soil. Another approach, which doesn't need any assumption regarding the granular matter fabric, was developed to interpret results from the jet erosion tests (JET) and the hole erosion tests (HET), and it is based on the power expended by the seepage flow (Marot *et al.*, 2011; 2012a). In a such approach, changes of hydraulic soil characteristics are implicitly taken into account through the flow power. Thus hydraulic loading and its evolution on one hand, and the soil response to this loading on the other hand are completely coupled.

Sterpi (2003) carried out several suffusion tests on samples of silty sand in order to investigate the quantity of eroded particles under controlled hydraulic gradients. A series of triaxial compression tests was also carried out to evaluate the effect of erosion on the mechanical behaviour of tested soil. These triaxial tests were performed on reconstituted samples with different fine particle contents to reproduce different stages of erosion development. The compression tests showed that the stiffness and the shear strength of the tested samples increase with a decreasing amount of fine particle content. In other words, it would suggest that stiffness and shear strength are not degraded by erosion of fine particles. More recently Chang and Zhang (2011), performed compression tests on samples actually subjected previously to erosion by suffusion and showed that shear strength and stiffness were, in their case, strongly reduced by the erosion process. Such results were also assessed from constitutive modellings (Scholtès *et al.*, 2010; Muir-Wood *et al.*, 2010). Consequently the influence of suffusion on mechanical properties of soils is still today an open question, and may strongly depend on the initial soil grading.

With the aim to characterize the hydraulic loading and the corresponding soil response a specific bench was designed (Sail *et al.*, 2011) and a series of tests was performed on mixtures of glass beads with two different fine particle contents. To consider different loading histories, the applied hydraulic gradient for each test was increased by stages according to different values of amplitude and duration. The variations of density and settlement of specimens due to suffusion process are studied and the influences of hydraulic loading history, percentage of fine particles and specimen length are investigated. The hydraulic

loading is characterized by fluid expended power and the corresponding erosion is characterized by the erosion rate. An expression of erosion rate related to fluid expended power is proposed and by time integration the cumulative eroded mass can be assessed.

## **2 Experimental device and test procedure**

The experimental device is configured to perform tests on cylindrical specimens (280 mm in diameter and height up to 600 mm), saturated and consolidated under oedometric conditions. Specimens are then subjected to a downward flow with a constant hydraulic gradient increased by steps. Although axial and radial stresses applied on the specimen cannot be controlled independently (as for instance in Chang and Zhang, 2013), an advantage of this device is to allow local measurements of density and interstitial pressure along longitudinal profiles.

The device and its equipments are illustrated in Figure 1. It comprises a rigid wall cell made of Plexiglas in order to observe specimen during testing time. This cell is equipped with fourteen pressure ports, all connected to a single pressure sensor via a multiplex unit (components are detailed in Alexis *et al.*, 2004, and in Figures 1 and 2). Such a system avoids measurement deviation between different pressure sensors. The device includes also an axial loading system which is composed of a pneumatic cylinder and a piston (itself composed of two perforated plates with a layer of gravel in between as represented in Figure 1, in order to diffuse the injected fluid uniformly at the top of the specimen). This axial loading system allows the measurement of the axial effective stress on the top of the specimen thanks to a load sensor. The specimen settlement is measured by a linear variable differential transducer (LVDT). The specimen is supported by a lower wire mesh itself fixed on a coarse and rigid mesh screen. The collecting system, downstream of the cell, includes an effluent tank with an overflow outlet (to control the downstream hydraulic head) and is equipped with a rotating sampling system containing 9 beakers for the sampling of eroded particles carried with the effluent. The detail of each component is reported in Sail *et al.* (2011).

Longitudinal profiles of specimen density are measured thanks to a gammadensitometric system. This system, detailed in Alexis *et al.* (2004) and shown in Figure 2, comprises a radioactive gamma-ray source and a scintillation counter on the opposite cell side. This system is bonded to a carriage moving in vertical direction thanks to an endless screw and a controlled electric motor. The position of the carriage is measured by a position transducer. According to a previous gauging data, a density calculator counts the scintillometer impulses

and calculates the mean density of the part of the specimen located 25 mm around the scintillation counter focal axis.

Figures 3a and 3b exemplify the positions of pressure ports used (labeled H6 or H4, L1 to L5 and R1 to R5), and density measurement stations (section S1 to S6), for specimen lengths of 250 mm and 450 mm respectively.

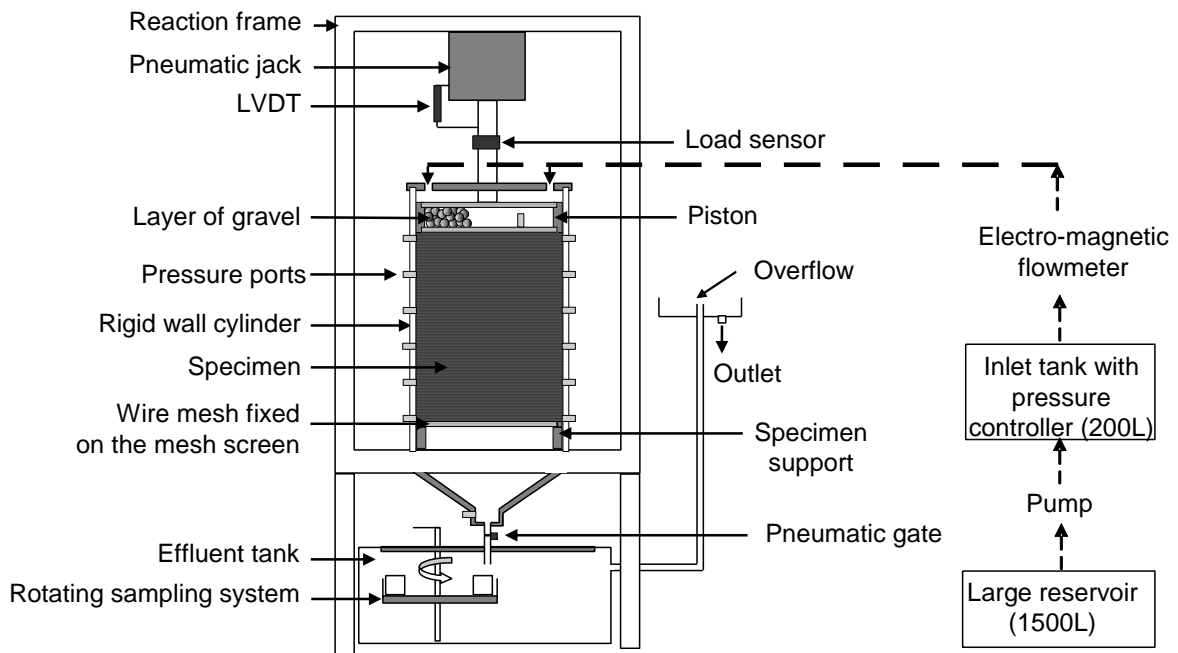


**Figure 1:** principle of cell, axial loading system, collecting system and hydraulic control system

Tested materials are two mixtures of glass beads. Glass beads have been chosen to avoid the influence of cohesion and grain angularity (Marot *et al.*, 2012b) on the erosion process, and also to perform comparisons with previously published results obtained by Moffat and Fannin (2006) with bead assemblies.

The two glass bead mixtures, G4-C (as named by Moffat and Fannin 2006) and G2-C, are composed of a coarse fraction C and a fine fraction F. Their grain size distributions are plotted in Figure 4, together with the grain size distribution of the coarse C and fine F fractions. According to Moffat and Fannin (2006), the fine fraction F is equivalent to a fine sand with a coefficient of uniformity  $C_u = 1.4$  and  $d_{85} = 0.19$  mm (where  $d_{85}$  is the sieve size for which 85 % of the soil mass is finer). Fraction C is equivalent to coarse sand with  $C_u = 1.7$  and  $d_{85} = 3.1$  mm.

G4-C mixture is a gap graded material composed of 40 % by mass of F and 60 % of C, whereas G2-C mixture contains 20 % of F and 80 % of C. Mixtures are obtained by mixing coarse and fine fractions during 3 minutes with 10 % of water content.

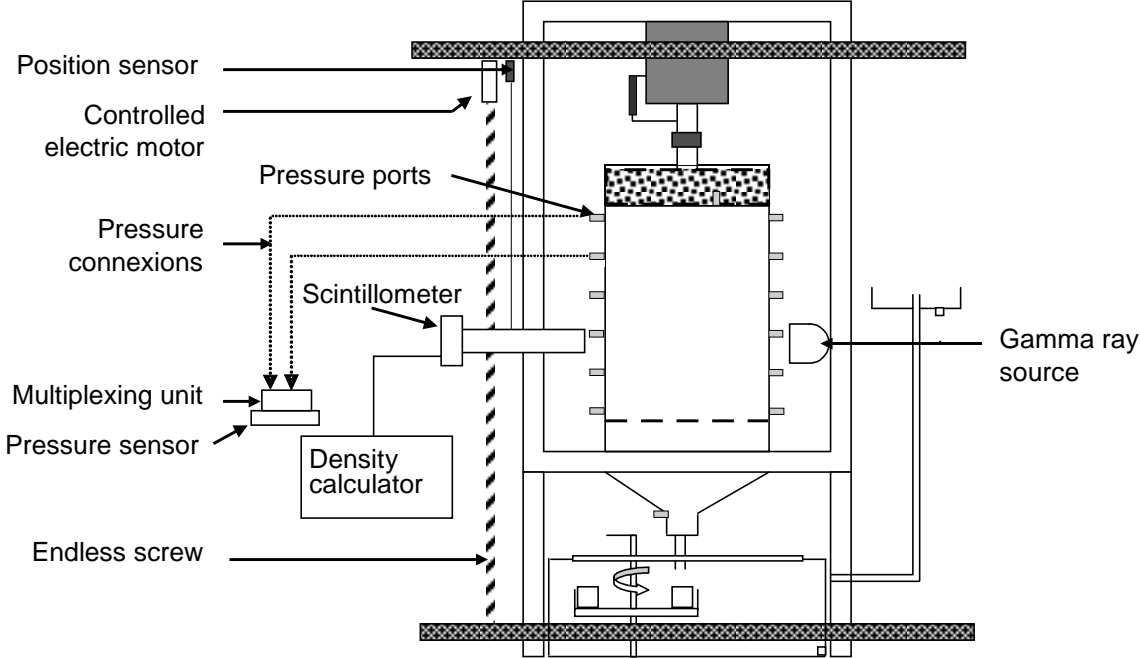


**Figure 2:** principle of gammadensitometric system and interstitial pressure measurement

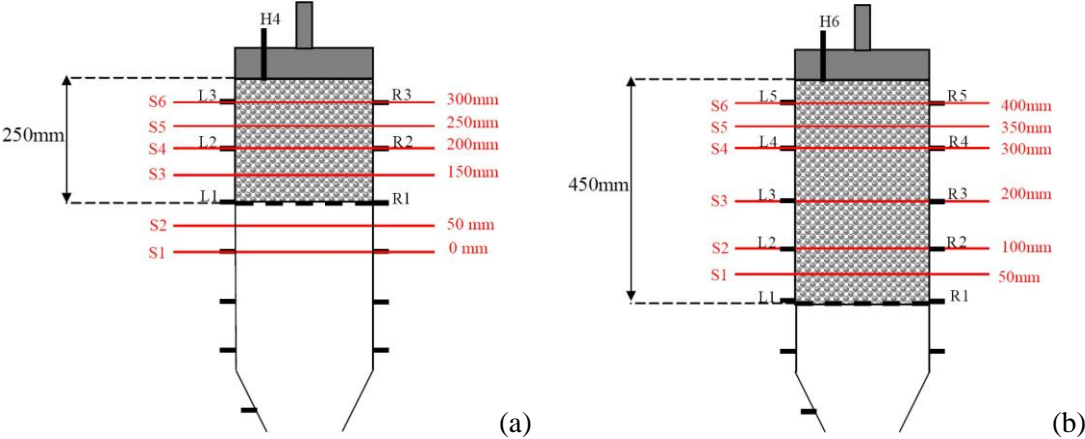


**Figure 3:** configuration of the cell of the oedo-permeameter (density measurement stations S1 to S6, and pressure port numbered L1, L2, ..., R1, R2, ...) with respect to the specimen lengths: 250 mm (a), or 450 mm (b)

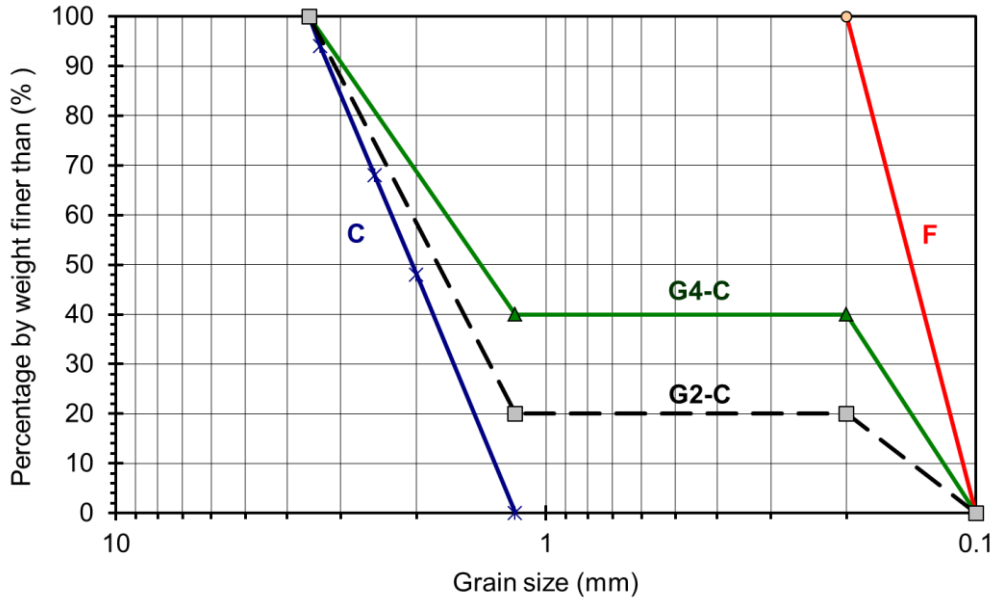


**Figure 4:** grains size distribution of glass bead mixtures G4-C and G2-C, and their coarse C and fine F fractions.

Each specimen is created by a technique of slurry deposition used by Moffat and Fannin (2006). The specimen is reconstituted on a lower wire mesh with a 1.25 mm pore opening size (see Figure 1) in order to allow the migration of fine particles only. The water level in the cell is initially set at 2 cm above wire mesh (i.e. the specimen support). Glass beads are then placed in several successive slurry-mixed layers (by ensuring a vanishing drop height to prevent mixture segregation), each one covered by the same 2 cm thin film of standing water, with the aim to maintain saturation of the material. The specimen is finally consolidated under a 25 kPa axial loading with drainage at the top and the bottom of the specimen. This axial loading is also maintained during the erosion test.

Eight tests were performed under different conditions characterized by four parameters: the initial fine particle content, the initial specimen length, the stage amplitude of global hydraulic gradient (defined as the ratio of the difference between upstream and downstream hydraulic heads to initial total specimen length), and the duration of each stage of global hydraulic gradient. The Table 1 shows the values of these parameters for each test and the initial values of average dry density  $\rho_d$  and hydraulic conductivity  $k_0$ . Successive steps of the global hydraulic gradient are detailed in Table 2 for each test.



Test	Percentage of fine particles (%)	Initial specimen length (mm)	Multi-stage of global hydraulic gradient $i$	Duration of stages (h)	Initial average dry density $\rho_d$ (g/cm <sup>3</sup> )	Initial hydraulic conductivity $k_0$ (m/s)
N1	40	250	1 – 2 – 3 – 3.2	1	1.81	$1.7 \cdot 10^{-4}$
N2	40	450	1 – 2 – 3 – 4 – 4.8	1	1.82	$1.2 \cdot 10^{-4}$
N3	40	450	1 – 2 – 3 – 3.7 – 4.7	1	1.86	$1.5 \cdot 10^{-4}$
N4	40	600	1 – 2 – 3 – 4.9 – 5.5	1	1.83	$1.2 \cdot 10^{-4}$
N5	40	250	0.1 – 0.2 – 0.4 – 0.8 – 1 – 2.2 – 3	1	1.79	$1.5 \cdot 10^{-4}$
N6	40	250	0.1 – 0.2 – 0.4 – 0.8 – 1	1 – 1 – 5 – 4 – 1	1.60	$3.8 \cdot 10^{-4}$
N7	20	250	0.1 – 0.2 – 0.4 – 0.5	1	1.83	$7.9 \cdot 10^{-4}$
N8	20	250	0.1 – 0.2 – 0.4	1	1.82	$16.0 \cdot 10^{-4}$

**Table 1** : main characteristics of performed tests

Test	Time range (min)								
	0-60	60-120	120-180	180-240	240-300	300-360	360-420	420-660	660-760
N1	1.0	2.0	3.0	3.2					
N2	1.0	2.0	3.0	4.0	4.8				
N3	1.0	2.0	3.0	3.7	4.7				
N4	1.0	2.0	3.0	4.9	5.5				
N5	0.1	0.2	0.4	0.8	1.0	2.2	3.0		
N6	0.1	0.2	0.4					0.8	1.0
N7	0.1	0.2	0.4	0.5					
N8	0.1	0.2	0.4						

**Table 2** : successive steps of the global hydraulic gradient  $i$  applied during each test with respect to the time elapsed from the test initiation

Figure 5 shows longitudinal profiles of specimen relative density (i.e. the ratio of the saturated sample density to the water density) measured with the gammadensitometric system after the consolidation step. A rather good homogeneity of specimen is obtained thanks to the slurry deposition technique with an average value of relative density of  $2.10 \pm 3.33 \%$ ; except for specimen of test N6, with a lower relative density of an average of 2.02, and a wider scattering. After specimen preparation, the loss of fine particles through the bottom wire mesh is measured and represents about 2.1 % of total fine mass. This affects mainly the downstream part of specimens as the relative density profile decreases in this part, in particular for specimens N5 to N8.

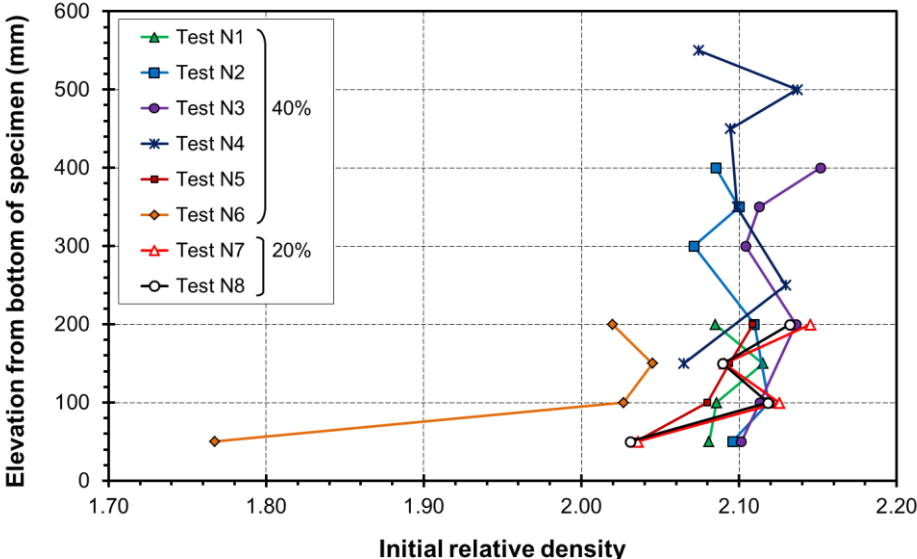


**Figure 5:** vertical profiles of relative density (ratio of the saturated sample density to the water density) at the beginning of tests

### 3 A two phases erosion process

The cumulative eroded mass is displayed in Figure 6a and 6b for mixture G4-C and G2-C respectively. Generally speaking, the eroded mass increases by steps, corresponding to the successive steps of applied hydraulic gradient (the rate of erosion is important at the beginning of the hydraulic step and then tends to decrease or even to vanish). Nevertheless, for all tests two main erosion phases are discernible. During the first phase, the cumulative eroded mass increases gradually with time, the erosion rate tends to vanish when the hydraulic gradient is kept constant, and the whole process is characterized by a low kinetic. On the other hand, during the second erosion phase, the erosion process is characterized by a

high kinetic: rate of eroded mass is much more important and does not decrease or vanish for a constant hydraulic gradient.

Post-test grading measurements showed that the suffusion process is rather diffused during the first phase and its development cannot be detected by visual observations from the beginning of tests as displayed in Figures 7a and 7b for G2-C mixture, and Figures 8a and 8b for G4-C.

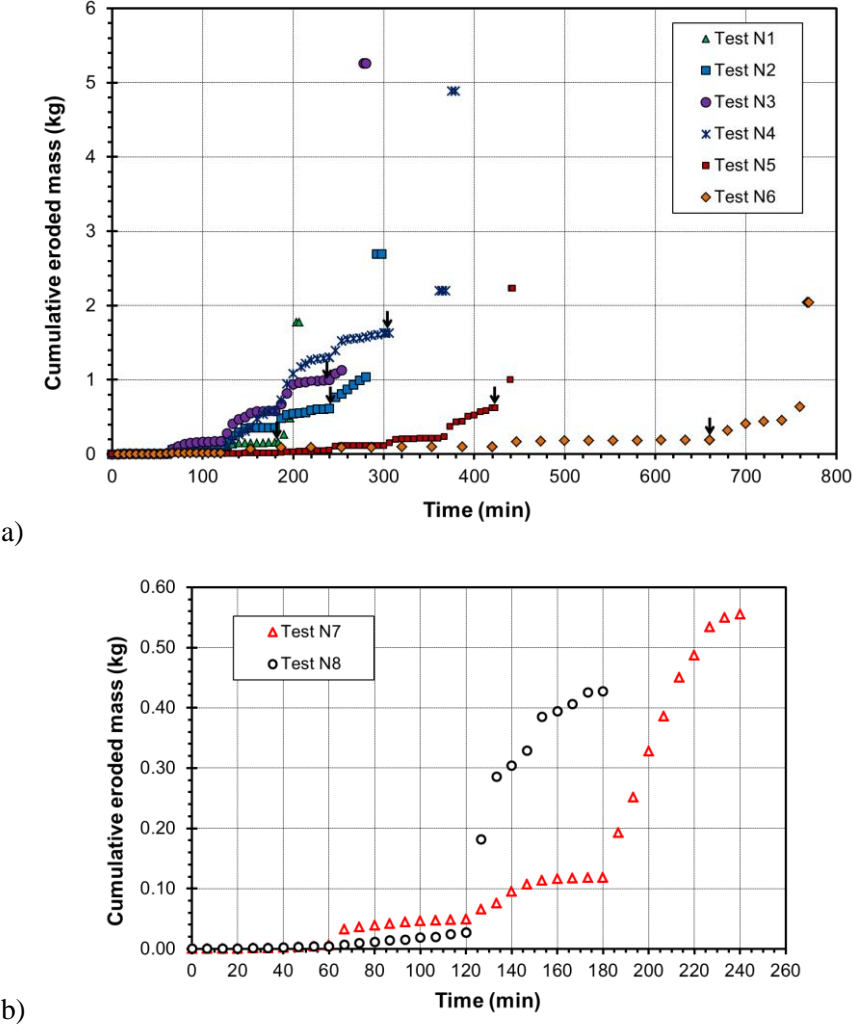


**Figure 6:** cumulative eroded mass for the G4-C mixture (a) and for the G2-C mixture (b), the arrows represent the time of initiation of the second erosion phase; hydraulic gradient applied at a given time can be identified by referring to Table 2

During the second erosion phase, effects of the suffusion process are visible to the naked eye. Zones where fine particles have been completely washed out (only the coarse fraction remains) develop from the top specimen and then progress in the downward direction. It is

worth noting that in the case of G2-C mixture, the whole specimen section seems to be concerned by this washing out process (see Figure 7c), whereas with G4-C mixture, fine particles are washed out only in a localized part of each tested specimen (see Figure 8c). Concerning the G4-C mixture, this second aggressive erosion phase was also observed by Moffat and Fannin (2006). They named it failure. Besides, it has been shown in Sail *et al.* (2011), that the suffusion process of the first erosion phase, always for G4-C mixture, is eventually accompanied locally by a filtration of some transported particles resulting in a partial clogging of the interstitial space and the generation of interstitial overpressure in the clogging zone. The second erosion phase is then initiated by the interstitial overpressure causing the blowout of the clogging, and washing out all the fine particles in the corresponding zone. For G2-C mixtures, such a development of interstitial overpressure has not been detected, either because the latter is too small, or because the second erosion phase may directly result from the increase of the global hydraulic gradient at the boundaries of specimens.

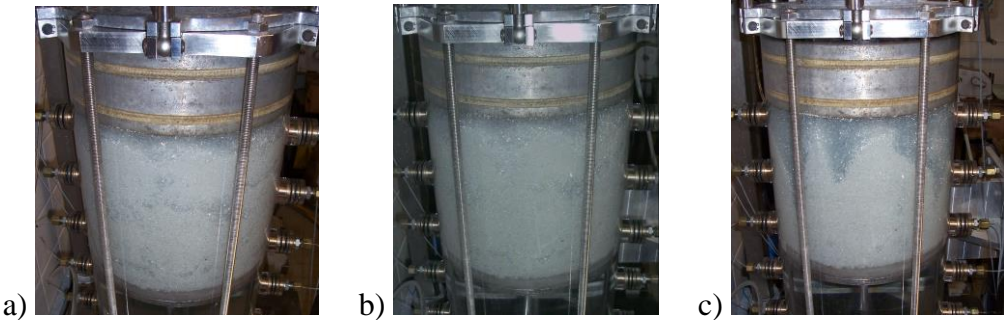


**Figure 7:** progression of internal erosion, test N7, G2-C mixture: a)  $t = 0$  and  $i = 0$ ; b)  $t = 180$  min and  $i = 0.4$ ; c)  $t = 240$  min and  $i = 0.5$

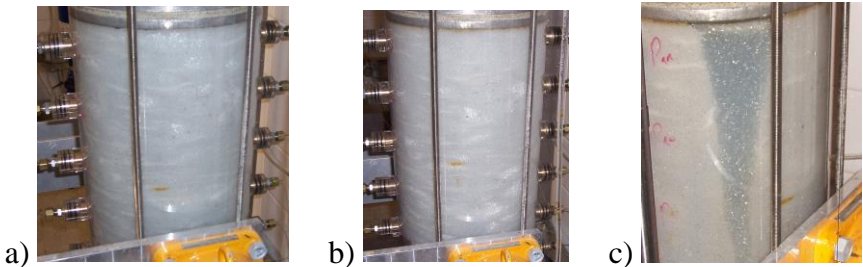


**Figure 8:** progression of internal erosion, test N2, G4-C mixture: a)  $t = 0$  and  $i = 0$ ; b)  $t = 240$  min and  $i = 4.0$ ; c)  $t = 286$  min and  $i = 4.8$

Figure 9 shows the instantaneous values of hydraulic conductivity. With 20 % of fine particles, initial hydraulic conductivity is  $7.9 \cdot 10^{-4}$  m/s and  $16 \cdot 10^{-4}$  m/s for tests N7 and N8 respectively. This slight discrepancy between initial hydraulic conductivity values for these two tests seems to emphasize the great influence of initial density: the less dense specimen is more permeable. In the same way, with 40 % of fine particles, hydraulic conductivity is initially between  $1.2 \cdot 10^{-4}$  m/s and  $1.7 \cdot 10^{-4}$  m/s for tests N1 to N5; whereas for test N6, characterized by a smaller initial density (see Figure 5 and Table 1), initial hydraulic conductivity is about  $3.8 \cdot 10^{-4}$  m/s.

The two different erosion phases can also be identified from the plot of hydraulic conductivity for both mixtures. For G2-C (Figure 9b), hydraulic conductivity increases first slowly (by a factor of about 1.8 over a time period from 2 to 3 hours), and then suddenly rises up to  $10^{-2}$  m/s (which represents an increase by a factor of 8 to 9 over a time period of about 30 min). All along tests on G4-C mixture (Figure 9a), hydraulic conductivity stays relatively constant, but finally strongly increases at the same time as the visual observation of the blowout initiation.

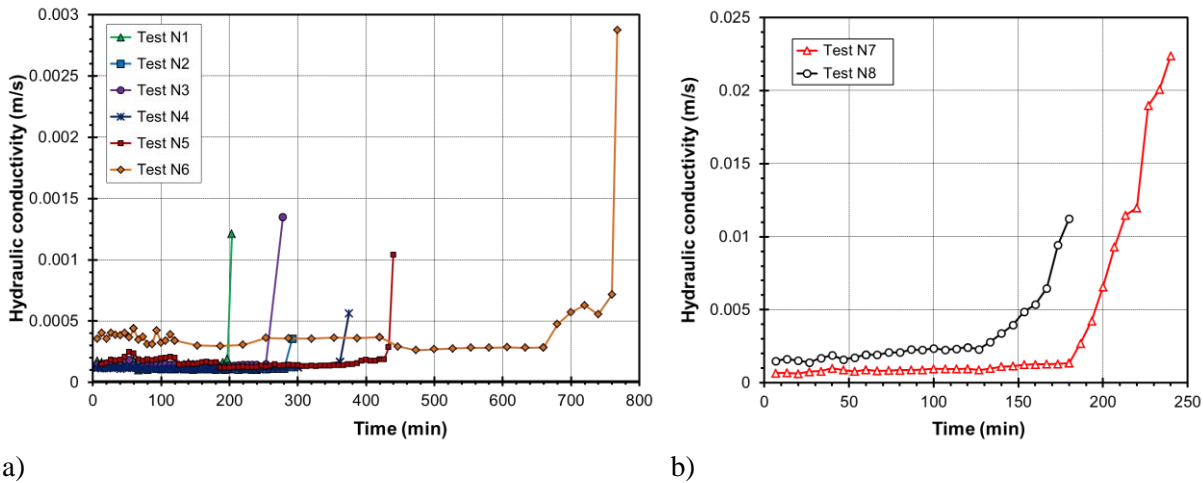


**Figure 9:** time series of hydraulic conductivity, for G4-C mixtures (a) and G2-C mixtures (b); hydraulic gradient applied at a given time can be identified by referring to Table 2

Different specimen lengths (250 mm for N1, 450 mm for N2 and N3, and 600 mm for N4) subjected to similar hydraulic loading histories were considered for the tests performed with the G4-C mixture. Even though the hydraulic gradient at initiation of the second erosion phase for these tests seems to increase with the specimen length (from  $i = 3.2$  for N1 to  $i = 5.5$  for N4), the influence of the length on the blowout initiation should be confirmed with additional repeatability tests.

We define the relative variations of density as  $(d - d_0)/d_0$ , where  $d_0$  and  $d$  are respectively the initial and the current densities. Figure 10 shows typical evolution of relative variation of density in the case of G2-C mixture (test N7) according to the different density stations identified in Figure 3a. During the first three fourth of test duration, suffusion process induces very small decrease (less than 0.5 %) of relative density all along the vertical profile of specimen. Then, a sharp decrease of relative density is measured at the same time as the important increase of hydraulic conductivity (Figure 9b). This density decrease concerns the whole specimen, but it is less marked in the specimen downstream part (section S3). In this bottom section, loss of fine seems to be partially counterbalanced by fine particles transported from the upstream part (as shown in Figure 7c, there is an important detachment and transport of fine particles in the top part of the sample). Here again the two erosion phases are clearly identifiable from the density changes of specimens.

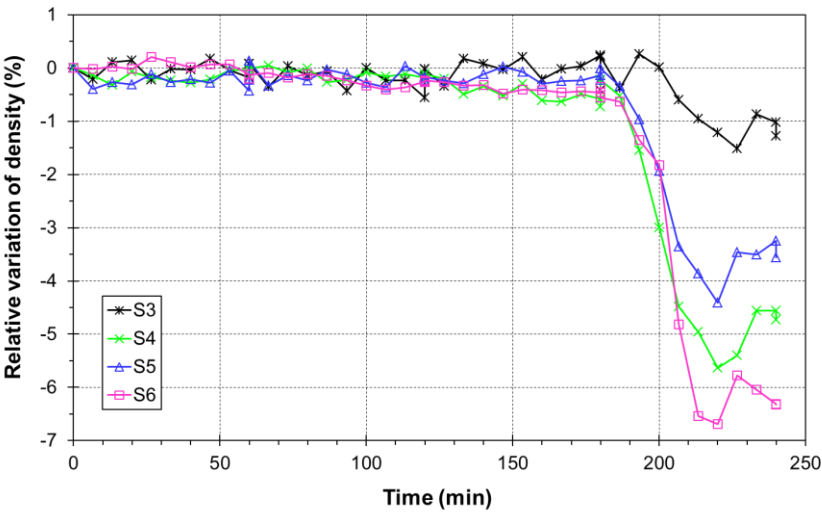


**Figure 10 :** relative variations of density for test N7 (G2-C mixture) at measurement stations S3 to S6 identified on the sketch in Figure 3a of the oedo-permeameter configured for a 250 mm length specimen

In the case of G4-C mixture (see Figure 11), two types of density variations are measured during tests: (i) a decrease of density in the downstream part of specimen (sections S1, S2 and S3), with a final relative change of about -1.4%; (ii) an increase of density in the upstream part (sections S4, S5 and S6) with a final relative change of +1.5% (for section S4), +3.7% (for S5) and +5.1% (for S6). In the specimen upstream part, the density increase starts before

the increase of hydraulic conductivity (presented in Figure 9) and the visual observation of blowout initiation, and is thus developing during the first erosion phase.

The gamma-ray radiations, used for density measurements, cover on the peripheral surface of the specimen a circular area with a radius of 25 mm (Sail *et al.*, 2011). As in this case of G4-C mixture, the second erosion phase is localized (Figure 8c), the sudden local drop of density related to the washing out of fine particles cannot be captured if the gammay-ray source is not in front of the localized eroded zone. Consequently the second erosion is not identifiable in times series of density (Figure 11), but has a strong influence on hydraulic conductivity as previously shown, by opening a preferential flow path.

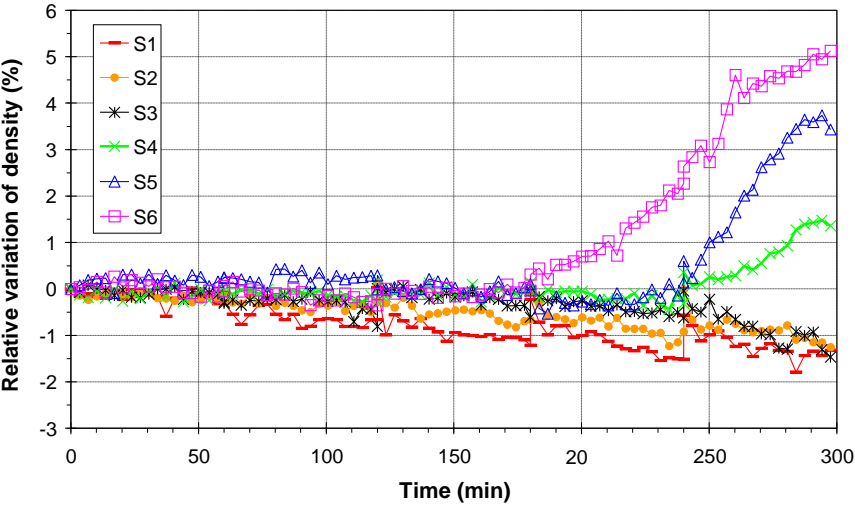


**Figure 11:** relative variations of density for test N2 (G4-C mixture) at measurement stations S3 to S6 identified on the sketch in Figure 3b of the oedo-permeameter configured for a 450 mm length specimen

Besides, for binary mixtures of particles there is an optimum fine particle content for which a maximum of density of the mixture is reached (the coarse particles form a continuous granular skeleton and fine particles exactly fill the voids of this coarse skeleton). The optimum content of fine particles is generally very roughly about 25-30 % (see for instance Vallejo, 2001; Lade & Yamamuro, 1997; Tong et al., 2012). Consequently it explains why, with an initial percentage of fine particles of 20%, the loss of particles is accompanied by a decrease of specimen density (the coarse particles initially form a continuous granular skeleton, and with erosion voids of the coarse skeleton are progressively emptied of the fine particles). On the other hand, with 40 % of fine particles, coarse particles are initially

“floating” within the fine fractions, and loss of fine particles allows a compaction of the coarse fraction and an increase of specimen density in the upstream part (Sail *et al.*, 2011). In the downstream part, loss of fines may be counterbalanced by fine particles transported from an upstream detachment zone.

Despite these differences between G2-C and G4-C specimens, general conclusions can be drawn. Changes of density for both mixtures seem to show that the first erosion phase concerns the whole specimen. Moreover the second erosion phase induces relatively high changing rates of hydraulic conductivity and density, whereas the first erosion phase seems to affect these parameters only at a low rate. Consequently, the detection of the first erosion phase may be complicated, due to its furtive development.

#### **4 Description of the eroded mass for the first erosion phase**

The development of suffusion is studied by the mean of relative eroded mass which is the ratio of the cumulative eroded mass, collected at the outlet of the specimen, to the initial mass of fine particles constituting the specimen. The relative eroded mass is plotted according to global hydraulic gradient in Figure 12 for all the tests. G2-C mixture appears more erodible than G4-C mixture as with G2-C mixture relative eroded mass reaches high values (from 5 % up to 8 %) for hydraulic gradients smaller than 0.5; whereas for G4-C mixture a relative eroded mass of 4 % is first reached for a hydraulic gradient of about 3. More generally, a given value of hydraulic gradient can correspond to a large range of relative eroded mass for G4-C and G2-C mixtures respectively. For example with hydraulic gradient 1, the relative eroded mass for G4-C mixture ranges from less than 0.04% for tests N1 to N4, 0.35% for test N5, to 1.65% for test N6 (a factor 10 is also observable concerning the relative eroded masses corresponding to the hydraulic gradient of 3). Consequently, although relative eroded mass increases with global hydraulic gradient, no clear relation can be proposed. The stage duration and the number of hydraulic loading stages seem to have an influence on suffusion development.



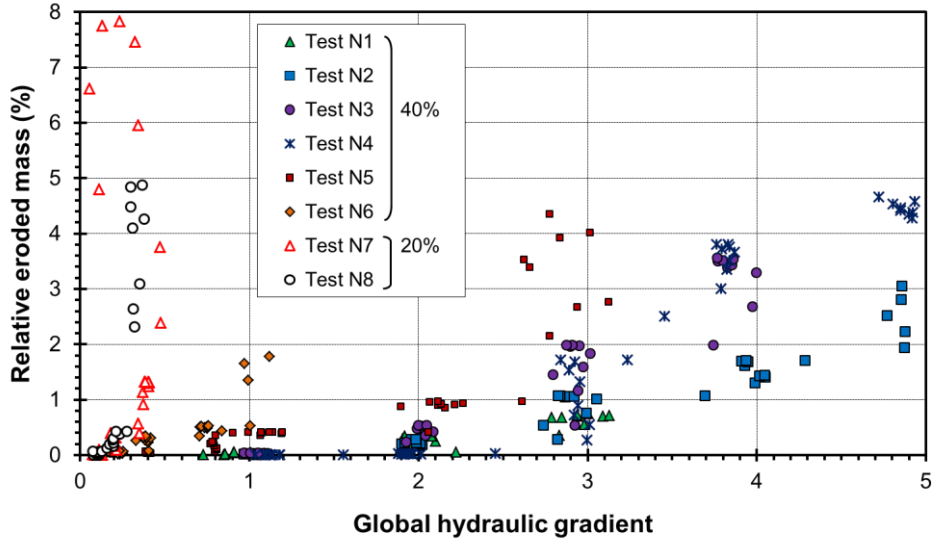


**Figure 12:** relative eroded mass vs global hydraulic gradient

Consequently, we suggest in the following to represent the hydraulic loading by the power expended by the fluid flow. Such approach was first proposed to interpret results from jet erosion tests and hole erosion tests by Marot *et al.* (2011), and then adapted to suffusion (Marot *et al.*, 2012a). The expression of the fluid flow power deduced from the energy conservation equation for the fluid phase, involves four assumptions according to Marot *et al.* (2011, 2012a): (i) the fluid temperature is constant, (ii) the system is adiabatic, (iii) a steady state flow is considered, and (iv) as the value of Reynolds number is indicating a laminar flow (Marot *et al.*, 2012a), it is assumed that energy is mainly dissipated by viscous shear at the direct vicinity of solid particles and is thus representative of solid-fluid interactions (Sibille *et al.*, 2014). Thanks to these assumptions, the flow power  $P_{flow}$  expended by the fluid to seep through a homogeneous soil volume can be expressed by:

$$P_{flow} = (\Delta p + \gamma_w \Delta z) Q \quad (1)$$

where  $\Delta p = p_A - p_B$  is the pressure drop between the upstream section A of the soil volume and the downstream one B;  $\gamma_w$  is the specific weight of water;  $\Delta z = z_A - z_B$ , with  $z_A$  and  $z_B$  the vertical coordinates of sections A and B respectively; and  $Q$  is the volumetric water flow rate.  $\Delta z > 0$  if the flow is in the downward direction, whereas  $\Delta z < 0$  for an upward flow. Finally the flow power reduces to  $Q \Delta P$  if the flow is horizontal.

In the following we consider for the G4-C mixture only the first erosion phase identified during the suffusion tests for which specimens and water seepage are rather homogeneous. In other words we discard the second erosion phase where the erosion process can develop in a strongly localized way. In this latter case, the application of the energetic approach proposed is not straightforward and would require a spatial discretization scheme. Regarding the G2-C mixture, both first and second erosion phases can be assumed homogeneous and are considered. Then, since we assume the specimen and the seepage to be homogenous, and in order to express data independently from specimen volumes, the analysis is conducted from the flow power per unit volume  $P_v$  (ratio of flow power to the specimen volume), and the erosion rate per unit volume  $\dot{m}_v$ , defined as:

$$\dot{m}_v = \frac{\Delta m_{eroded}}{V \Delta t} \quad (2)$$

where  $\Delta m_{eroded}$  is the dry mass of eroded particles collected during a duration  $\Delta t$ , and  $V$  is the volume of the specimen. Erosion rate per unit volume is plotted according to the flow power per unit volume in Figure 13 for tests performed with G4-C mixture, and in Figure 14 for G2-C mixture tests. For each test, the different stages of global hydraulic gradient are distinguished by using different symbols.

The case of test N2 is displayed alone in Figure 15 to exemplify the analysis detailed below. For each stage, the flow power is rather constant (because of the low permeability changes) and plots form vertical lines. The highest mass erosion rates (represented by the top of each vertical line and circled in Figure 15) are obtained respectively at the beginning of each hydraulic gradient stage. Then during stages, erosion rates decrease. Vertical lines are followed in the downward direction (Figure 15) because of the reduction of available beads within the specimen which can be detached and transported under the hydraulic loading applied (some beads may require a higher hydraulic loading to be detached due to their important interlocking with the granular skeleton (Bonelli and Marot, 2011)), and also because of the possible development of filtration of transported beads within the specimen.

In a first time we characterize the erosion rate at the initiation of each stage, which is assumed to be representative of the detachment step independently of the quantity of potentially erodible beads and of a possible filtration step. This is represented by the upper limit envelop of data plotted in Figures 13 and 14 and approximated here with the power law:

$$\dot{m}_v^{upper\ limit} = \alpha_{ref} P_v^b \quad (3)$$

with  $\alpha_{ref} = 0.003$  and  $b = 0.8$  for G4-C mixture; and  $\alpha_{ref} = 0.007$  and  $b = 1.5$  for G2-C mixture.  $\alpha_{ref}$  and  $b$  are parameters intrinsic to the material tested and representing its erodibility.

Then, the decrease of erosion rate during each stage emphasizes the necessity to take into account the history of hydraulic loading, i.e., the amplitude but also the duration of each stage. With such objective, the flow energy per unit volume  $\Delta E_v$  cumulated from the initiation of each hydraulic stage is defined as the time integration of the instantaneous flow power per unit volume from the initiation time  $t_{init}$  of the considered stage:

$$\Delta E_v = \int_{t_{init}}^{t > t_{init}} P_v dt \quad (4)$$

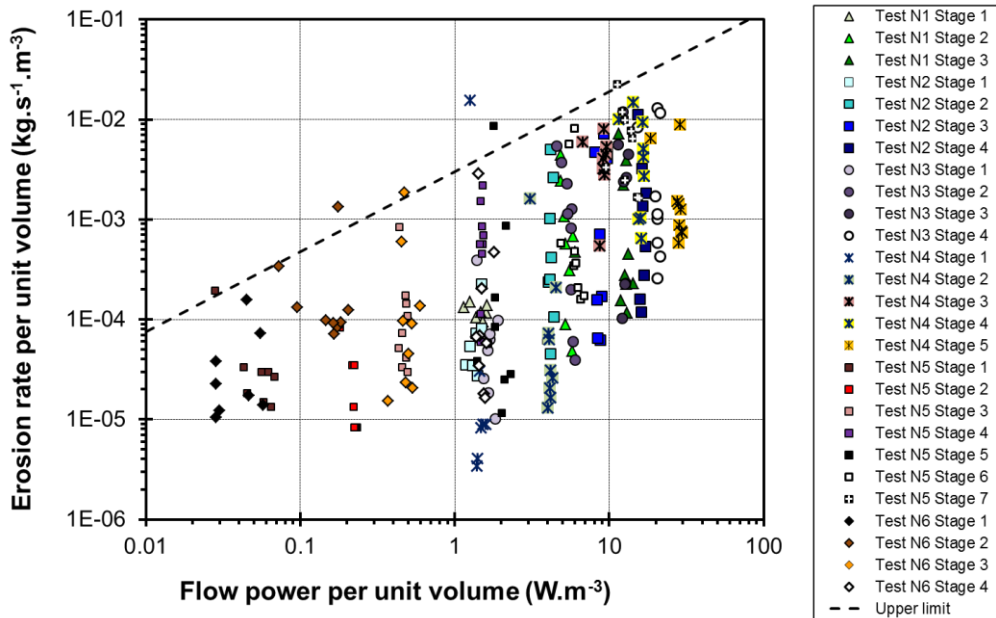


**Figure 13:** identification of the maximum erosion rate per unit volume as a function of the flow power per unit volume (G4-C mixture).

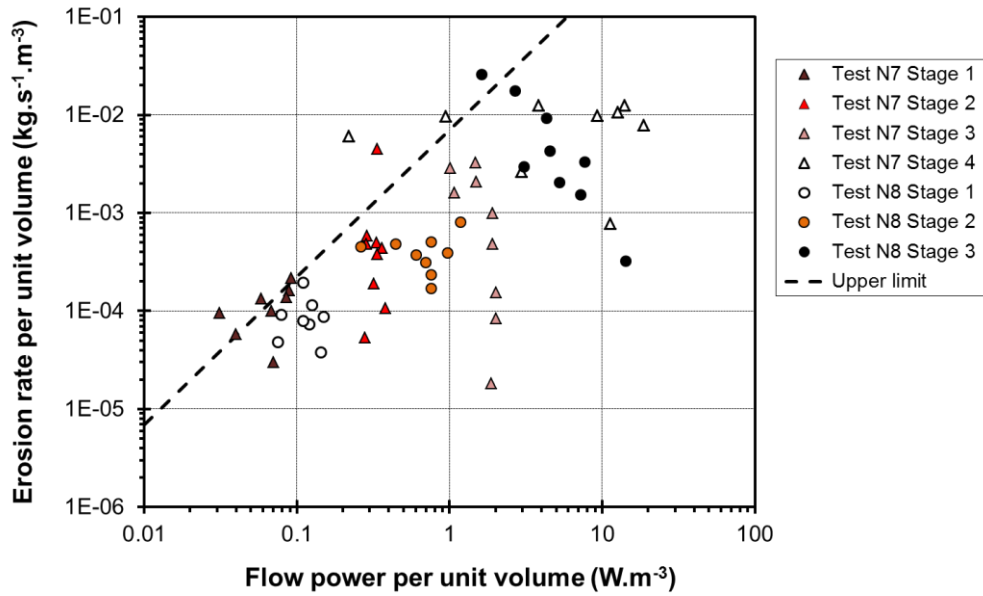


**Figure 14:** identification of the maximum erosion rate per unit volume as a function of the flow power per unit volume (G2-C mixture).

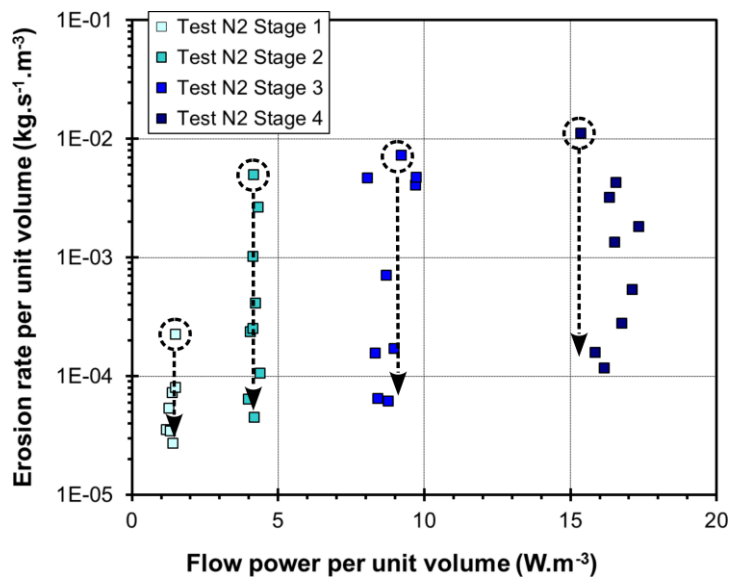


**Figure 15:** decrease of the erosion rate for an almost constant flow power for each hydraulic gradient stage, case of test N2 as an example.

$\Delta E_v$  constitutes here a history parameter. The mass erosion rate is finally expressed as:

$$\dot{m}_v = \alpha_{ref} \left( \frac{1}{\frac{\Delta E_v}{P_v t^*} + 1} \right) P_v^b \quad (5)$$

where  $t^*$  is a characteristic time relative to the tested material.

The laboratory test results show that changes of hydraulic conductivity remain quite low here, particularly during the first erosion phase (Figure 9). Thus for the sake of simplicity we assume that the hydraulic conductivity remains constant and equal to its initial value  $k_0$ . In addition, settlements of the specimen (discussed in the next section) are also neglected and specimen length is assumed constant and equal to  $\Delta z_0$ . Then, thanks to the Darcy law, the flow power per unit volume can be written as:

$$P_v = k_0 \left( \frac{\Delta p^2}{\gamma_w \Delta z_0^2} + \frac{2\Delta p}{\Delta z_0} + \gamma_w \right) \quad (6)$$

Finally, by combining Equations (4) to (6), the erosion rate per unit volume  $\dot{m}_v$  can be computed at any time. Four parameters are required  $\alpha_{ref}$ ,  $b$ ,  $t^*$ , and  $k_0$ ; and  $\Delta p$  describes the hydraulic loading applied to the specimen.

To assess the validity of the description proposed, the cumulative eroded mass  $m$  defined as:

$$m = V \int_0^t \dot{m}_v dt \quad (7)$$

and deduced from equations 4 to 6, is compared with the collected mass measured during laboratory tests, in Figure 16 and 17 for G4-C and G2-C mixtures respectively. The initial hydraulic conductivity  $k_0$  (given in Table 1) has been directly measured for all the tests, and the characteristic time  $t^*$  has been fitted from test N2 for G4-C mixture ( $t^* = 130$  s), and from test N7 for G2-C mixture ( $t^* = 1000$  s), other tests constituting consequently validation cases.

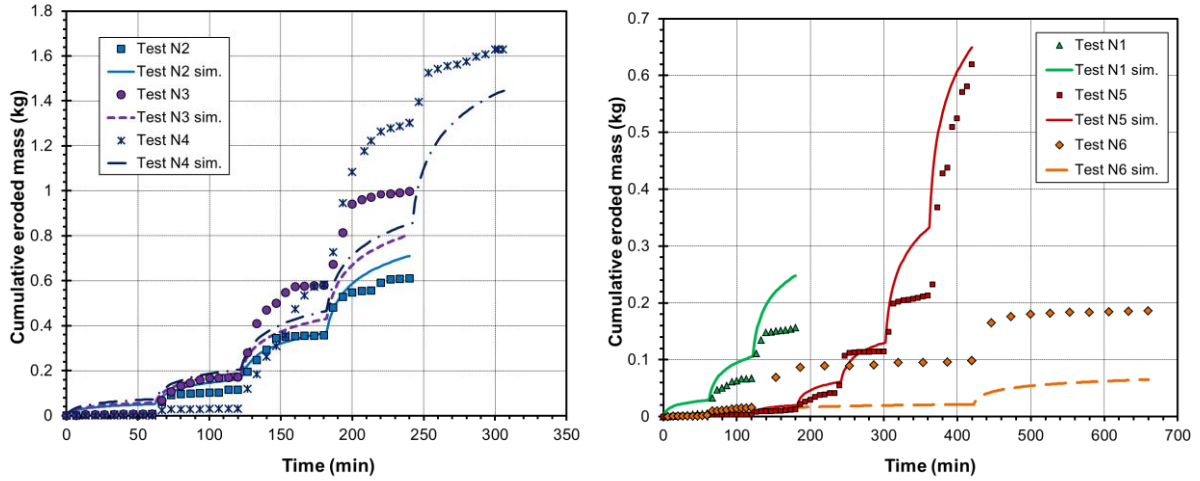


**Figure 16:** comparison of cumulative eroded masses during the first erosion phase for G4-C mixture, between laboratory tests (symbols) and simulated data (continuous lines); tests N2 to N4 are displayed on the left, whereas tests N1, N5 and N6 are displayed on the right

Concerning the G4-C mixture the description proposed is able to capture the main features of the erosion process for the calibration test N2, but also for the other validation tests differing from the specimen size or the hydraulic loading history. However the prediction of eroded mass is not totally in agreement with the experimental data. Although tests N2 and N3 have been performed with the same parameters (see Table 1) and thus stand for the repeatability of tests, the cumulative mass of particles collected is about 25 % larger for test N2 than N3. Obviously the model is not able to describe such a difference since the input parameters are identical, or at least almost identical (for instance the hydraulic conductivity for N2 is  $k_0 = 1.24 \cdot 10^{-4}$  m/s, whereas  $k_0 = 1.50 \cdot 10^{-4}$  m/s for test N3). Consequently due to the discrepancies between the experimental data, it is difficult to conclude here about the ability of prediction of this rather simple model. Actually repeatability of suffusion tests generally constitutes a drawback, poorly discussed in the literature and from authors' knowledge no repeatability results concerning suffusion tests have been published so far.

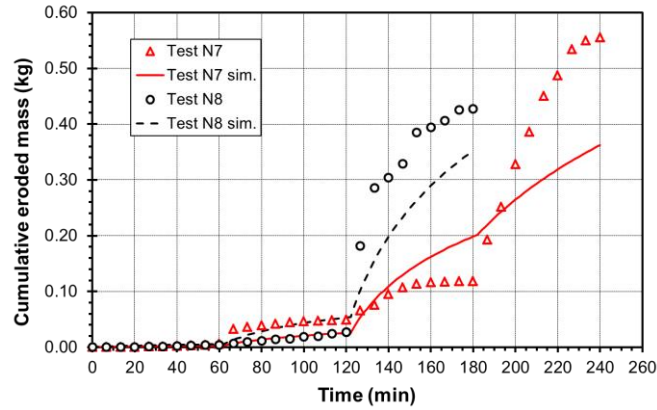


**Figure 17:** comparison of cumulative eroded masses for G2-C mixture, between laboratory tests (symbols) and simulated data (continuous lines)

All the model parameters identified for the G2-C mixture ( $\alpha_{ref}$ ,  $b$ ,  $t^*$ ) are larger than those identified for the G4-C mixture. This difference reflects the fact that G2-C mixture is more sensitive to erosion by suffusion than G4-C, as shown from the brief interpretation based on hydraulic gradient and presented in Figure 12. This more important erodibility is related to fine particles being more easily detached from the granular skeleton (reflected by larger values of  $\alpha_{ref}$  and  $b$ ); but also by a filtration step much less developed (reflected by a greater characteristic time  $t^*$ ). Indeed the lack of interstitial overpressure seems to show that no clear clogging happens for G2-C mixtures.

Predicted eroded masses for G2-C mixture are compared with measured ones in Figure 17 for tests N7 and N8. Tests N7 and N8 are identical excepted the initial hydraulic conductivity (see Table 1) for N8 being two times as large as permeability for N7, due to a slight variation in specimen preparation. Even if once again the model gives only the general trend, the main influence of this difference in the initial hydraulic conductivity seems to be described. Finally the underestimation of the eroded mass for the last hydraulic gradient stage for both tests N7 and N8 could be explained by the increase of the permeability during this last stage, and not taken into account with the simulations.

## 5 Settlements induced by suffusion

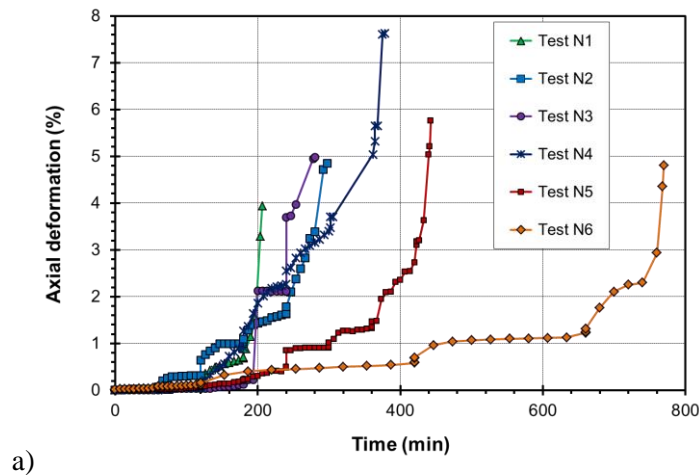
In order to characterize settlements and volume variations induced by suffusion, time series of axial deformation are plotted in Figure 18. The axial deformation is negligible during nearly total duration of G2-C mixture tests and finally presents a sharp increase in the last few

minutes, to reach 1.7 % for test N8 and 3.9 % for test N7. Since the G2-C mixture includes only 20 % of fine particles, these latter are almost not involved in the shear strength, the coarse beads forming a quasi-continuous granular skeleton. Consequently fine particles can be removed, up to a given amount, without any effect on specimen settlement. Voids of the coarse fraction are just partially emptied of fines. It is only during the second erosion phase, when fine particles are importantly washed out, that the coarse granular skeleton is impacted (granular skeleton involving however some fines beads), and specimen settles.

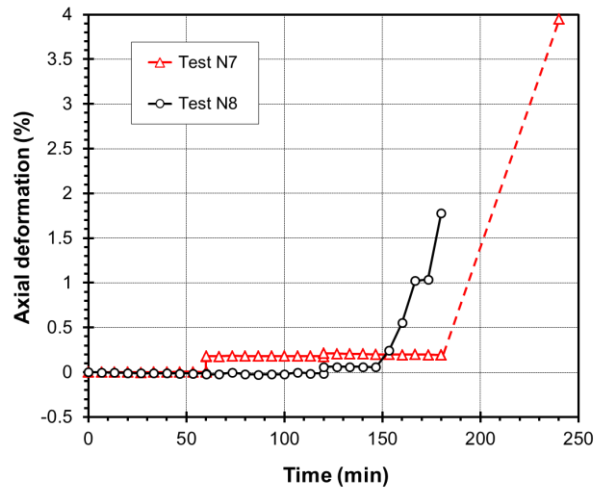
Concerning G4-C mixture, axial deformation slightly increases relatively slowly and gradually during the first half test duration, and finally increases much more rapidly in second half of test duration to reach maximum values comprised between 3.9 % (test N1) and 7.7 % (test N4). It is worth noting that for G4-C mixture, the beginning of large rise of axial deformation can appear up to hundred minutes before the second erosion phase characterized by a strong blowout of fine particles (identified with arrows in Figure 6a). Thus the first erosion phase of this erosion by suffusion seems to have a significant effect on the settlement G4-C specimens, even if the kinetic of the erosion process is relatively slow during this phase. This can be explained by the more important fine fraction and coarse beads floating, a least partially, in the fine ones. Then any removal of fine particles will result in a settlement of the specimen.

To improve the understanding of the settlement in the case of the G4-C mixture, the volume change of specimens (computed as the product between the settlement height and the area of the specimen cross section) are compared with an estimation of the bulk volume  $V_{bulk}$  occupied by eroded particles when they were in the specimen.  $V_{bulk}$  is directly deduced from the initial average dry density  $\rho_d$  (given in Table 1) and the cumulative eroded mass  $m$ :

$$V_{bulk} = \frac{m}{\rho_d} \quad (8)$$







b)

**Figure 18:** axial deformation vs time, for G4-C mixtures (a) and G2-C mixtures (b)

The bulk volume of eroded particles in terms of specimen volume change is displayed in Figure 19. If settlements are directly due to the loss of volume occupied by eroded particles, plots should follow the bisector line of the diagram. This is approximately the case except for test N3 with an almost nil volume change at the beginning of the test while erosion develops. This is due to the piston, initially stuck; but finally it follows the specimen settlement and the plot reaches the bisector line. Nevertheless plots are globally located slightly below the bisector line meaning that the single reduction of the specimen volume by the bulk volume occupied by eroded particles is not enough to explain the total settlement. The removal of fine particles offers the possibility for the remaining beads to compact (at least for the coarse fraction, in the upper part of the specimen as shown in Figure 11) leading to an additional settlement. Finally, at the very end of tests, plots are well above the bisector line (such points are not shown in Figure 19 for tests N3 and N4 because of the corresponding high values of  $V_{bulk}$ , about  $2700 \text{ cm}^3$ ). These last points correspond to the second erosion phase which is localized for G4-C mixture. Hence axial load is transferred on the section of the specimen not concerned by the second erosion phase, and global settlement is partially limited (even if important local settlement may develop, but not measurable with the piston).

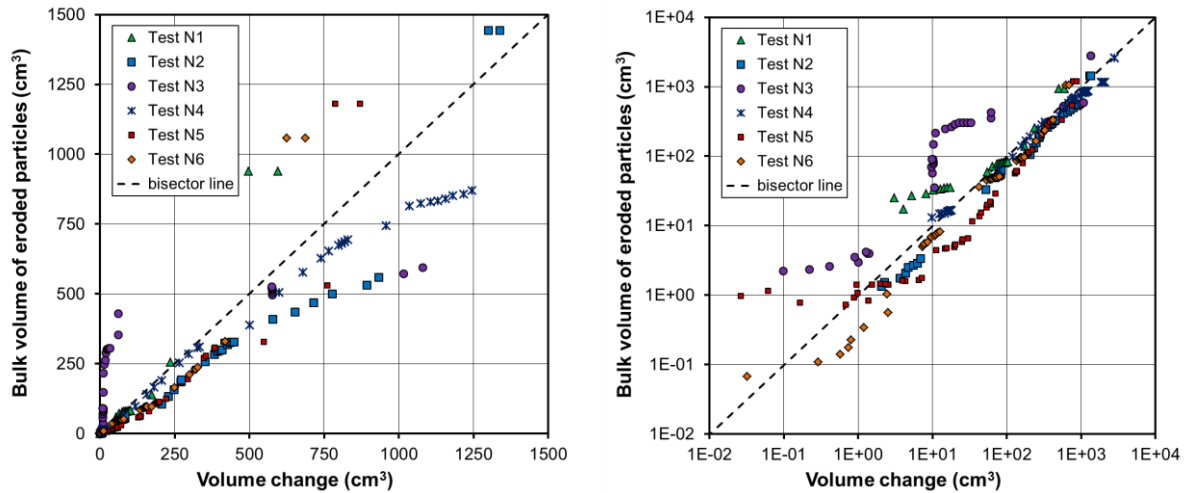


**Figure 19:** estimation for the G4-C mixture of the bulk volume occupied by eroded particles collected in terms of the change of volume of the specimen, linear scale on the left and logarithmic scale on the right

All these observations show that development of erosion by suffusion can induce specimen settlements even during the first erosion phase, where kinetic and eroded particles remain relatively moderate.

Concerning the G2-C mixture, the initial lack of settlement could lead to a misleading safe feeling in an engineering context concerning for instance a soil structure. In this case, important settlement may suddenly occur without any early warning signs. For G4-C mixture, response of the granular is more gradual and a rough estimation of the volume change can be deduced from the eroded mass.

## 5 Conclusion

Eight internal erosion tests on gap graded glass bead specimens were performed by using a large oedo-permeameter device. The cylindrical specimens contained an initial percentage of fine particles of 20% or 40% (corresponding mixtures are named G2-C and G4-C respectively) and with an initial length comprised between 250 mm and 600 mm. The influence of the hydraulic loading was investigated by increasing the controlled hydraulic gradient with different amplitudes and stage durations. The tests reveal that the erosion process is constituted here by a first suffusion phase concerning the whole specimen and inducing slight evolutions of hydraulic conductivity and specimen density, depending on the

initial percentage of fine particles. Although the suffusion development may be difficult to detect in situ, in an engineering context for instance, it has to be considered with attention as it can evolve toward a second phase of erosion by suffusion characterized by a blowout and an important washing out of fine particles inducing both a large settlement of specimen (up to an axial deformation of 7-8 %), and a relatively strong increase of the hydraulic conductivity. Thus the suffusion characterization and detection could take a great importance in order to prevent disorders relative to strong deformations of the considered structure (as a dike or a dam), or a strong increase of the seepage flow rate through this structure.

With such objective, the erosion rate by suffusion has been investigated according to the power expended by the seepage flow through the specimen. A rather simple phenomenological model involving four parameters to describe the mass of eroded particle (reaching the outlet of the specimen) during the suffusion process has been proposed. It is able to capture the main features observed experimentally during these tests composed of several hydraulic loading stages, and requires at least such a single multi-stage test to be calibrated.

Finally mechanical consequences of suffusion in terms of induced settlements have been investigated. It is shown that development of settlement is strongly dependent on the material grading and may be quite sudden, without early sign warning for the G2-C mixture. Concerning the G4-C mixture, volume changes and settlements can be estimated in a first approximation from the mass of eroded particles.

These descriptions and conclusions concerning erosion by suffusion are based on idealized materials constituted of glass beads and their application to natural soil would require further studies.

## References

- Alexis, A., Le Bras, G., Thomas, P. (2004). Experimental bench for study of settling-consolidation soil formation. *Geotechnical Testing Journal*, **27**: 557-567.
- Bendahmane, F., Marot, D., Alexis, A. (2008). Experimental parametric study of suffusion and backward erosion. *Journal of Geotechnical and Geoenvironmental Engineering*, **134**: 57-67.
- Bonelli, S. (Editor) (2012). Erosion in geomechanics applied to dams and levees, ISTE – Wiley.

- Bonelli, S. and Marot, D. (2011). Micromechanical modeling of internal erosion. *European Journal of Environmental and Civil Engineering*, **15**: 1207-1224.
- Burenkova, V.V. (1993). Assessment of suffusion in noncohesive and graded soils. Proc. 1<sup>st</sup> Conf Geo-Filters, Karlsruhe, Germany, Balkema, Rotterdam, The Netherlands, pp. 357-360.
- Chang, D.S., and Zhang, L.M. (2011). A stress-controlled erosion apparatus for studying internal erosion in soils. *Geotechnical Testing Journal*, **34**(6): 579-589.
- Chang D.S., and Zhang, L.M. (2013). Critical hydraulic gradients of internal erosion under complex stress states. *Journal of Geotechnical and Geoenvironmental Engineering*, **139**(9), 1454-1467.
- Fell, R., Fry, J.J. (2007). Internal erosion of dams and their foundations. Taylor & Francis Publisher.
- Kenney, T.C., Lau, D. (1985). Internal stability of granular filters. *Canadian Geotechnical Journal*, **22**: 215-225.
- Kovacs, G. (1981). Seepage hydraulic. Elsevier Scientific Publishing Co, Amsterdam.
- Lade, P. V., and Yamamuro, J. A. (1997). Effects of non plastic fines on static liquefaction of sands. *Canadian Geotechnical Journal*, **34**(6): 918-928.
- Li, M. (2008). Seepage induced instability in widely graded soils. PhD Thesis, University of British Columbia, Vancouver, Canada.
- Li, M., Fannin, J. (2008). Comparison of two criteria for internal stability of granular soil. *Canadian Geotechnical Journal*, **45**: 1303-1309.
- Marot, D., Bendahmane, F., Rosquoët, F., Alexis, A. (2009). Internal flow effects on isotropic confined sand-clay mixtures. *Soil & Sediment Contamination*, **18**: 294-306.
- Marot, D., Regazzoni, P.L., Wahl, T. (2011). Energy based method for providing soil surface erodibility rankings. *Journal of Geotechnical and Geoenvironmental Engineering*, **137**: 1290-1294.
- Marot, D., Le, V.D., Garnier, J., Thorel, L., Audrain, P. (2012a). Study of scale effect in an internal erosion mechanism. *European Journal of Environmental and Civil Engineering*, **16**: 1-19.
- Marot, D., Bendahmane, F., Nguyen, H.H. (2012b). Influence of angularity of coarse fraction grains on internal erosion process. *La Houille Blanche*, **6**: 47-53.
- Muir Wood D., Maeda K., Nukudani E. (2010). *Modelling mechanical consequences of erosion*. *Géotechnique*, **60**(6): 447-457.
- Moffat, R., Fannin, R.J. (2006). A large permeameter for study of internal stability in cohesionless soils. *Geotechnical Testing Journal*, **29**: 1-7.

- Moffat R. and Herrera P. (2014). Hydromechanical model for internal erosion and its relationship with the stress transmitted by the finer soil fraction. *Acta Geotechnica*, online first published 2014. DOI: 10.1007/s11440-014-0326-z
- Perzmaier, S. (2007). Hydraulic criteria for internal erosion in cohesionless soil. In *Internal erosion of dams and their Foundations*. Editors R. Fell and J.J. Fry. Taylor & Francis, pp. 179-190.
- Reddi, L.N., Lee, I., Bonala, M.V.S. (2000). Comparison of internal and surface erosion using flow pump test on a sand-kaolinite mixture. *Geotechnical Testing Journal*, **23**: 116-122.
- Sail, Y., Marot, D., Sibille, L., Alexis, A. (2011). Suffusion tests on cohesionless granular matter. *European Journal of Environmental and Civil Engineering*, **15**: 799-817.
- Scholtès, L., Hicher, P.Y., Sibille, L. (2010). Multiscale approaches to describe mechanical responses induced by particle removal in granular materials, *Comptes Rendus Mécanique (CRAS)*, **338**(10-11):627-638.
- Shire T. and O’Sullivan C. (2013). Micromechanical assessment of an internal stability criterion, *Acta Geotechnica*, **8**:81-90. DOI:10.1007/s11440-012-0176-5
- Sibille L., Lominé L., Poullain P., Sail Y., Marot D. (2014). Internal erosion in granular media: direct numerical simulations and energy interpretation. *Hydrological Processes*, online first published 14 Oct 2014. DOI:10.1002/hyp.10351
- Skempton, A.W., Brogan, J.M. (1994). Experiments on piping in sandy gravels. *Géotechnique* **44**: 449-460.
- Sterpi, D. (2003). Effects of the erosion and transport of fine particles due to seepage flow. *International Journal of Geomechanics*, **3**: 111-122.
- Tong A.T., Catalano E., and Chareyre B. (2012) Pore-Scale Flow Simulations: Model predictions compared with experiments on bi-dispersed granular assemblies. *Oil & Gas Science and Technology*, **67**(5): 743-752. DOI:10.2516/ogst/2012032.
- Vallejo, L.E. (2001). Interpretation of the limits in shear strength in binary granular mixtures. *Canadian Geotechnical Journal*, **38**: 1097-1104.
- Vincens E., Witt K.J., Homberg U. (2014) Approaches to determine the constriction size distribution for understanding filtration phenomena in granular materials, *Acta Geotechnica*, online first published 2014. DOI: 10.1007/s11440-014-0308-1
- Wan, C.F., Fell, R. (2008). Assessing the potential of internal instability and suffusion in embankment dams and their foundations. *Journal of Geotechnical and Geoenvironmental Engineering*, **134**: 401-407.